SSC21-VI-08

Mission concept for demonstrating small-spacecraft true anomaly estimation using Millisecond X-Ray Pulsars

Anant Kandala[1], Aashka Oza[2], Bharath Saiguhan, Shreya Mishra
Priyadarshnam Hari, Samir Mandal, Harsh Simha M S
Indian Institute of Space Science and Technology
Thiruvananthapuram, India; [1]+919711101451
[1]278anant@gmail.com
[1]Currently at Human Space Flight Center, Indian Space Research Organisation
[2]Currently at Satellite Applications Center, Indian Space Research Organisation

ABSTRACT

Navigation based on X-ray pulsars was first suggested in 1981[1] for deep space navigation as an alternative to the conventional Deep Space Network (DSN) which is inaccurate at large distances from the Earth. This idea was recently demonstrated[2] using the NICER/SEXTANT instrument onboard the ISS. X-ray pulsar-based navigation is of of great interest as it eliminates the reliance on Earth-based systems, and is yet to be implemented as an autonomous navigation system for deep space missions. For the purpose of navigation, X-ray millisecond pulsars are the most appropriate celestial sources. They emit unique, stable and periodic radiation that exhibits high timing stability comparable to atomic clocks, thus making them suitable as navigational beacons. The phase difference between the pulsar's pulse profile obtained at the satellite and a reference profile is tied to the position of the satellite with respect to the chosen reference location, typically considered to be the Solar System Barycenter (SSB). Measurements from at least four pulsars are required to estimate the 3D position, velocity, and time of the satellite. This article describes a small satellite mission concept being developed at the Small-spacecraft Systems and PAyload CEntre (SSPACE) at the Indian Institute of Space Science and Technology (IIST) that aims to demonstrate navigation in space using X-ray millisecond pulsars. The satellite contains a miniaturized X-ray timing detector payload, which extracts accurate pulse profiles from detected pulsar signals. A mission-specific algorithm is developed that uses measurements from a single pulsar to estimate only the true anomaly of the satellite, since given the orbital insertion, the other orbital elements are assumed to be stationary. Additionally, the process of pulsar selection is presented, where pulsars are ranked according to the weighted parameters of stable time periods, visibility from the chosen orbital configuration, and high signal-to-noise ratio with respect to the diffuse X-ray background. This is followed by details of the instrument design and concept of operations of this technology demonstration mission. The article concludes with an overview of the systems architecture of the small-satellite, which has a standard 6U CubeSat form factor and details regarding the various subsystems including the On Board Computer, Electrical Power System, Communication system, and Attitude Determination and Control System are discussed. A successful demonstration of this mission will pave the way for future small-satellite missions, where 3D position estimation can be carried out using multiple X-ray pulsar detectors.

Introduction

Small satellites have relatively low budget and development time that allows the design of missions with higher risks, making them excellent candidates for deep space missions that aim to explore unknown/potentially dangerous environments. However, navigation in such missions is a challenging task due to the power, size and cost constraints imposed by small satellites. The current interplanetary small satellites typically access the Deep Space Network (DSN) for navigation, which is both time and power intensive. As distance from the earth increases, the accuracy of earth based navigation systems also reduces drastically, making them unsuitable for deep space missions. In addition, the Direct to Earth (DTE) link time of the deep space satellites is less with long time gaps between consecutive links. This further increases the need for autonomous navigation systems in deep space missions. Millisecond pulsars provide a precise method for position estimation as they produce periodic beacon signals with timing accuracy rivaling atomic clocks.[3] By comparing the pulse profile of these beacons measured at the

satellite with the pulse profile at a reference location, the position of the satellite can be estimated. The XNavSat mission is being developed by the Small-spacecraft Systems and PAyload CEntre(SSPACE) at the Indian Institute of Space Science and Technology, Kerala, India, to demonstrate the feasibility of navigation in space using X-ray Pulsar measurements. This mission is a technology demonstration that aims to calculate the true anomaly of the satellite using a novel and compact instrument capable of making accurate X-ray Pulsar timing measurements. The objective of the mission is to estimate the true anomaly of the satellite in real time, assuming the remaining orbital elements of the satellite are known. This one-dimensional estimation problem, if successfully demonstrated, can then be extended to complete position estimation using multiple X-ray pulsars, in the future.

Navigation using X-ray Pulsars

Pulsars are highly magnetized neutron stars, rotating at a very high speed about their spin axis. The rotation accelerates charged particles which emit electromagnetic radiation along the magnetic field axis. In case of misalignment of the spin and magnetic axes, the radiation produced appears as a sequence of pulses to an observer not on the spin axis. Hence for the observer the pulsar emits periodic radiation. It has been observed that pulsars have extremely stable rotation periods. Pulsars are observed in radio, X-ray, visible and gamma-ray bands of the electromagnetic spectrum, of which the most efficient regime for autonomous navigation using pulsars is the X-ray band. This is so because of the small detector size requirement and the fact that a larger proportion of the emitted energy lies in the X-ray band. In order to compute the navigation solution, the photons from the pulsar are time-tagged at the detector. The exposure time decides the number of cycles of the pulsar recorded. These photon time-tags are folded to one pulsar period. The folded times (between 0 and P, where P is the pulsar period) are binned, and the histogram thus produced is normalized between 0 to 1. The resulting normalized histogram is the pulse profile. In order to produce a pulse profile that would be observed at the Solar System Barycenter (the reference pulse profile), a time transfer has to be done in the above process to shift the times of arrival observed at the satellite (observer) to those at the SSB (reference). A comparison between the received pulse profile at the satellite's position with the reference pulse profiles (for various pulsars) can be used to autonomously calculate the 3D position of the satellite with respect to the SSB. Thus, the basic idea behind XNAV is to use these stable pulsars to navigate. Specifically, the pulse profile generated from the detector's data is compared to the reference profile to find the time delay, t_d between the two. Using this time delay, and given the pulsar's characteristics (such as the period, direction vector with respect to the SSB etc.), one can compute the range in the direction of the pulsar. As an extension of this methodology, one can find the 3-dimensional position of the satellite by recursively estimating ranges in the directions of several pulsars. For the purposes of this paper, the relation between the 3-dimensional position and the true anomaly of the satellite is made use of, so as to estimate the latter. The procedure of estimating the true anomaly using the measurements from only one pulsar are explained in the subsequent sections.

Source Selection for X-ray Pulsar Navigation

For the purposes of navigating with the help of X-ray pulsars, a source ranking process was carried out. Here, first the list of all pulsars known to emit periodically in the X-ray regime was accumulated from literature,[4] along with their respective pulse properties such as period, flux, sky positions etc. Then for each pulsar on this list, assuming the satellite was in a circular, sun-synchronous orbit with a semi-major axis of 500 km (with all other Keplerian orbital elements are assumed to be 0 for simplicity), the visibility to the satellite was ascertained. This was done by utilising the following condition[4] :

$$|\pi - \arccos(\hat{\mathbf{n}} \cdot \hat{\mathbf{r}}_{SC/B})| \leq \arccos\left(\frac{\sqrt{r_{SC/B}^2 - R_B^2}}{r_{SC/B}}\right) \tag{1}$$

where $\mathbf{r}(t)_{SC/B}$ is the position of the spacecraft with respect to a celestial body (here, Earth) at a particular time t, R_B is the radius of the body in consideration and $\hat{n}$ is the direction cosine of the pulsar in question. If the condition is true, then for those time instants, the pulsar will be occulted by the body in consideration. Otherwise, the pulsar will be visible unless some other body (which is unaccounted for) is occulting the source. For the purposes of this analysis, the visibility of the pulsars from the source list was ascertained by splitting one orbital period into 50 segments and checking the validity of the condition above, once in each of the segments. Only the Earth was considered as the main occulting body.

Along the same lines, simulations were carried out to ascertain the times when each source attained a sun angle greater than 30°. These would be considered "good" observing times, since the source would not be affected drastically by the radiation of the Sun. For this analysis, the positions of the satellite with respect to the SSB were computed and positions of the Sun were queried from the DE-430 ephemeris, using which the sun angle for each pulsar as viewed from the satellite was computed for each time segment. The interval from 1st January, 2021 - 31st December, 2022 was considered as a representative time frame for the calculations.

Furthermore, using Aladin[5] , X-ray sources within 0.5°, 1° and 6° of the pulsars in question were queried from the 3rd XMM-Newton Enhanced catalog[6] (3XMMe), the 2nd Release of the Chandra Source Catalog[7,8] (CSCv2), and the ROSAT All Sky Survey Faint Source Catalog[9] (RASS-FSC). This was used to ascertain the amount of background noise to be expected from non-pulsar sources. Although some pulsars have hundreds of sources which are brighter than 10% of the pulsar's flux in the 1-10 keV range, it is expected that upon epoch folding to make the pulse profile, the only noise that these extraneous sources will contribute will be the diffuse X-ray background. This assumption simplifies further analysis, but more careful extraneous source analysis needs to be done to ensure that minimal quasi-periodic noise is contributed. However, from this analysis of the background sources it was arrived upon that a pointing accuracy at least of 1° or better is required to be able to sufficiently capture photons from the pulsar of interest.

Finally, using metrics derived from the above analyses, the various pulsars in the Pulsar Source Catalog were ranked. These metrics are as follows:

- Pulsar visibility fraction, $\mathcal{F}_{\text{vis}}$: this is computed as the ratio of time segments the pulsar is visible in to the total number of time segments considered (here, 50). If this fraction is close to 1, the pulsar is ranked higher.

- Favourable Sun-source separation fraction, $\mathcal{F}_{\text{Sun-source}}$: this is computed as the ratio of time segments when the pulsar is greater than 30° away on the sky to the total number of time segments. A higher ranked pulsar has this value close to 1.

- Background source statistics: this information is taken into account in the ranking by considering how many background sources have a 1-10 keV flux of :

  1. Greater than 1/100 the pulsar's flux, within a circular sky region centered on the pulsar and 0.5°, 1° and 6° in radius. The corresponding counts are denoted as $\mathcal{N}_{>0.01}(r)$ where r is the angular sky radius considered.
  2. Greater than 10 times the pulsar's flux, with the same specifications as above. These counts are denoted as $\mathcal{N}_{>10}(r)$.

The 'score' for a pulsar is computed according to these metrics using the following heuristic:

$$\text{Score} = 50(\mathcal{F}_{\text{vis}}+\mathcal{F}_{\text{Sun-source}})-20\cdot\mathcal{N}_{>10}-\frac{\mathcal{N}_{>0.01}}{50} \quad (2)$$

This score was then used to rank the pulsars in the pulsar source list, and the Crab pulsar (PSR J0534+2200) was thus chosen as the main target for this mission, due to both its high 'score' as well as brightness in the 1-10 keV energy range.

Constraining Detector Specifications

In order to better guide detector design and structure, a constraint is imposed that the observation of a particular pulsar is done at a signal-to-noise ratio above a certain threshold. This ensures that the photons detected from a particular pulsar are significant, even if the underlying noise is non-gaussian. For this purpose, the threshold SNR is set to 5, i.e. observations with an SNR > 5 are deemed statistically significant. From the literature,[4] the SNR (denoted by S) for a detection is given as:

$$\begin{aligned} \text{S} &= \frac{N_{S_{\text{pulsed}}}}{\sigma_{\text{noise}}} \\ &= \frac{N_{S_{\text{pulsed}}}}{\sqrt{(N_B + N_{S_{\text{non-pulsed}}})_{\text{duty cycle}} + N_{S_{\text{pulsed}}}}} \\ &= \frac{F_x A p_f \Delta t_{\text{obs}}}{\sqrt{[B_X + F_X(1-p_f)](A\Delta t_{\text{obs}} d) + F_x A p_f \Delta t_{\text{obs}}}} \end{aligned} \quad (3)$$

where:

- A is the detector area
- Δt_{obs} is the observation time
- p_f, the pulsed fraction, is the percentage of the source flux which is pulsed
- d is the duty cycle of the pulse, which is the duration of the pulse profile occupied by the pulse component relative to the pulsar period. For a pulsar with period P and pulse component of width W, $d = W/P$.

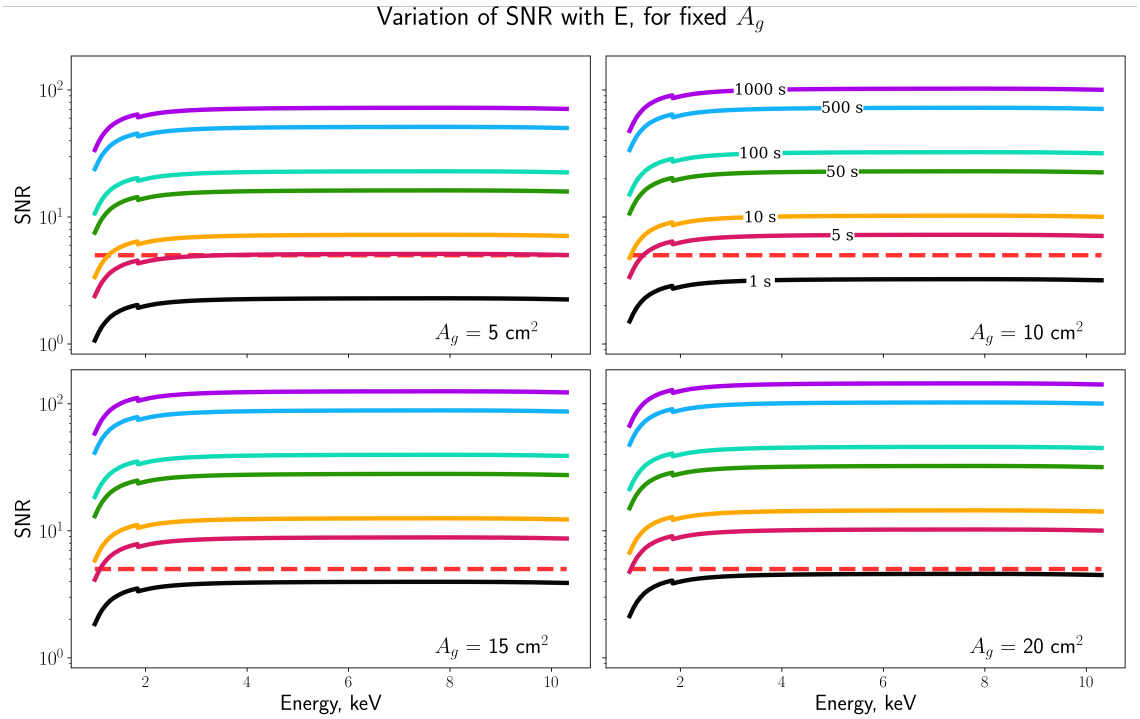

Figure 1: Simulated SNR(E, $\Delta t_{\mathbf{obs}}$) considering the Amptek FAST SDD, for fixed geometric areas = 5, 10, 15, 20 cm^2. The dashed red line marks the SNR = 5 threshold. Lines are color-coded according to the $\Delta t_{\mathbf{obs}}$ value considered, as in the top right panel.

- F_X is the observed source X-ray flux
- B_X is the background X-ray flux
- N_{pulsed} is the pulsed component of the source flux, and σ_{noise} is the one sigma detection error

Note that this equation implicitly depends on the detector parameters, such as the (effective) area and observation time. Thus, this equation can be used in tandem with the aforementioned SNR threshold to constrain the detector specifications. Due to their high quantum efficiency in the energy range of interest (1-10 keV), Silicon Drift Detectors (SDDs) are chosen as the base detector type. These can be arranged in a grid or mosaic, as required, to increase the effective area available for detecting photons. In order to decide how many of these detectors would be required to meet the SNR threshold constraint, along with the effect of the observation time, a trade-off study was carried out with SNR being the primary variable. Its variation with the detector geometric area, quantum efficiency and observation time was studied. For this, the quantum efficiency of the Amptek FAST SDD[10] was used from which the effective area of the detector was calculated as:

$$A_{eff}(E) = \epsilon(E) \cdot A_{geom} \tag{4}$$

where $A_{eff}(E)$ is the effective area of the detector as a function of energy E, $\epsilon(E)$ is the quantum efficiency of the detector at that energy E and A_{geom} is the geometric area of the detector. This effective area was used to compute the SNR from equation 3, thus giving SNR as a function of both E and Δt_{obs}. For simplifying the description, only results related to the Crab pulsar (PSR J0534+2200) trade off study are presented here (other pulsars were considered, specifically the top six ranked pulsars from the Pulsar Source Catalog described in this work, but all other pulsars required large effective detector areas or prohibitively large observation times, both of which would require design goals tangential to the current body of work). As can be seen from the figure 1, if one considers the average SNR over the 1-10 keV range, one obtains an SNR > 5 for any effective detector area above 5 cm^2 and an observation time above 50 s. However, for the sake of instrument design, a detector geometric area of 5 cm^2 and an integration time of 100 s was fixed. Each Amptek FAST SDD has a 70 mm^2 detector, which is further collimated to an active geometric area of 50 mm^2. Thus this design choice implies that roughly 10 detectors will be required to achieve the SNR threshold. Furthermore, one should note that these estimates are

only indicative and for the purpose of guiding instrument design. Subsequent analyses and simulations need to be done to validate the assumptions made here and to include effects of other important factors. Such simulations would have to include the effects of background noise sources not considered here (such as the diffuse X-ray background, stray cosmic X-ray photons etc), instrumental effects (such as instrumental jitter, off-axis viewing effects etc) and other environmental effects.

Instrument Design

The main objective of the instrument is to extract timing information from detected photons of the pulsar source, use it to generate the required pulse profile and implement a navigation algorithm using the pulse profile. Figure 2(a) shows the preliminary CAD model of the instrument. The instrument occupies approximately 2U volume in the satellite. The various components of the instrument are also labelled in figure 2(b). Based on the SNR considerations explained in the previous section, the instrument consists of ten 70 mm^2 FAST SDDs along with their PA130 preamplifier developed by Amptek. External multilayer hollow-tube collimaters of length 12 cm (approx.) are added to each of the detectors. The collimaters allow only axial or par-axial rays to enter the detector and also prevent the diffuse X-ray photon noise from entering the detector. The instrument consist of three in-house designed PCBs namely, the **Analog Processing Unit (APU)**, **Digital Processing Unit (DPU)**, and **Power Conditioning Unit (PCU)**. Figure 3 shows the functional block diagram of the instrument, that highlights the interconnections between the various units. This section describes the functionality of each of the units of the instrument.

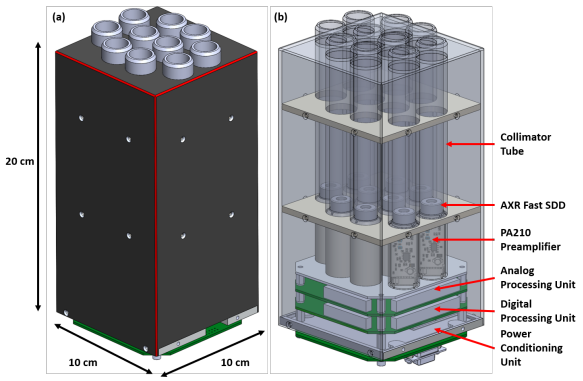

Figure 2: Preliminary CAD Model (a) Outer Structure (b) Inner Components

Amptek FAST SDD and Preamplifier

The detector proposed is off the shelf, 70 mm^2 FAST SDD developed by Amptek in a TO-8 package. The Amptek FAST SDD includes an inbuilt CMOS charge sensitive preamplifier and thermoelectric cooler inside the TO-8 package. The silicon drift detector is similar to Si-PIN photodiode except for the unique electrode structure, offering a better energy resolution and count rate. Integration of the transistor in SDD reduces total input capacitance dramatically, thus reducing electronic noise and enhancing speed of signal processing. The proposed detector has an active area of 50 mm^2, with total geometric area of 70 mm^2. A multilayer internal collimator is mounted on the detector element to mask the edges of active volume and this assembly is capped by a cover with a very thin Be window to allow soft X-rays.

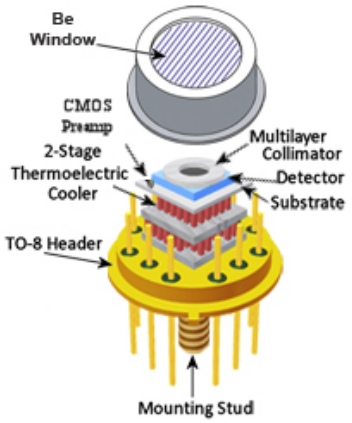

Figure 4: Silicon Drift Detector (SDD)

Analog Processing Unit (APU)

The output from the detector package is given to an Analog Processing Unit built in-house which has a signal conditioning circuit comprising of a fast transimpedance amplifier, constant fraction discriminator and comparator. The fast transimpedance amplifier enhances the timing characteristic of the incoming pulse. The pulse given as output after transimpedance amplifier has a faster return rate to zero after peak, therefore making extraction of peak time more accessible by differentiation.

Following this, a constant fraction discriminator (CFD) circuit is used which gives zero crossing at a constant fraction of pulse amplitude, thus virtually eliminating amplitude walk. Since the pulses received from the SDD will have varying amplitudes, proportional to incident photon energy, it is essential to design a signal processing system which over-

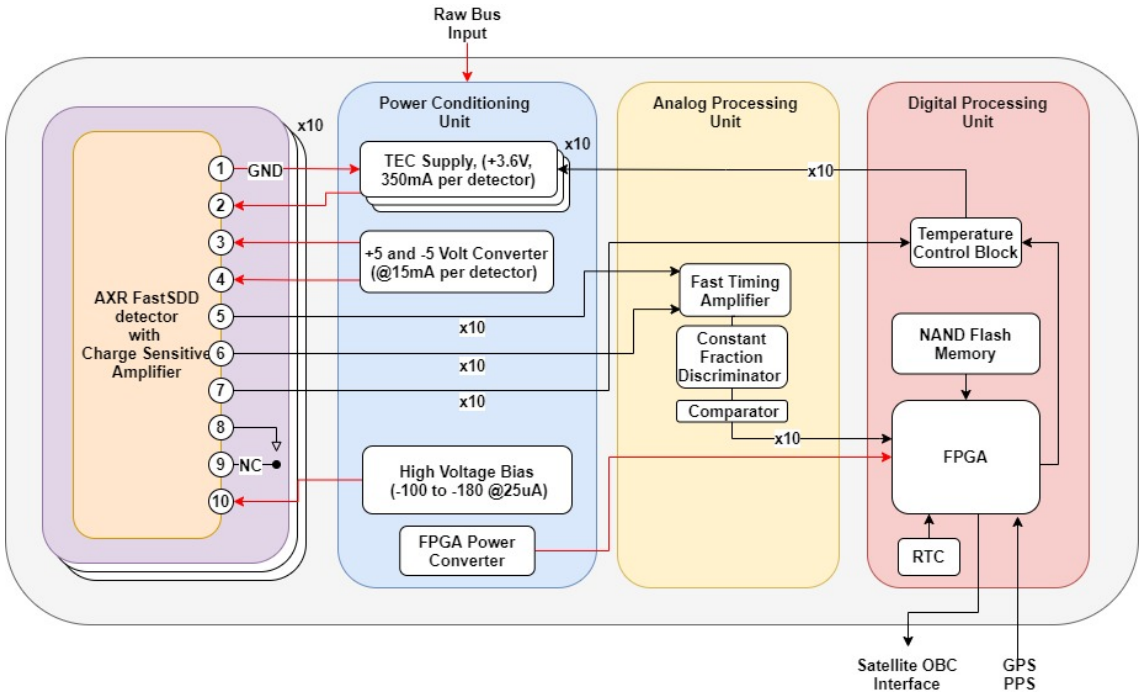

Figure 3: Instrument Functional Block Diagram

comes all such issues. The CFD takes the fast timing amplifier output and splits the signal in two, one part is attenuated by some fraction (say, f) while the other part is inverted and delayed. The two pulses are summed together to give out a bipolar pulse, for which the zero crossing occurs whenever the pulse reaches a fraction (f) of its peak amplitude. The bipolar pulse is sent through a comparator to detect the zero crossing and generate a logic pulse. The signal is thus digitised and sent to the Digital Processing Unit (DPU).

Power Conditioning Unit (PCU)

The Power Conditioning Unit consists of DC-DC converters that are used for converting satellite raw bus voltage to different regulated levels as required by the instrument. It consists of 3.6V regulators for the Thermoelectric Cooler (TEC) power supply of each of the SDDs. In order to maintain the detector temperature, the TEC power supply is controlled by the FPGA in the DPU, using a temperature sensor in the detector as feedback for implementing a closed loop control system. The PCU consists of a +5V and -5V converter to power the preamplifier of the detector. In order to provide a high voltage bias to the SDD, the PCU consists of high voltage regulated power outputs (in the range of -100V to -180V). The PCU also consists of the power converters required to power the various components in the APU as well as the DPU.

Digital Processing Unit (DPU)

The Digital Processing Unit consists of an System on Chip (SoC) FPGA that is used to detect and time-tag the comparator output from the Analog Processing Unit. The DPU consists of a high resolution Quartz based Real Time Counter (RTC), which is used to time tag the X-ray photon count values. The RTC value is also periodically synced with the GPS Pulse Per Second (PPS) signal, which is provided as an external input from the satellite. The DPU consists of non-volatile NAND flash memory that is used to store the time tagged instrument measurements. The memory can also be used to store reference pulse profile data as well as ephemeris data which would be required for implementing the navigation algorithm. The SoC FPGA in the DPU produces a time tagged array of X-ray photon count values. This array can either be sent to the satellite's On Board Computer for downlinking or can be used to implement navigation algorithm in the FPGA itself. For this mission, the FPGA is planned to implement the algorithm to estimate the true anomaly of the satellite using time tagged X-Ray photon count values. Further details of the algorithm are presented in the next section.

Satellite True Anomaly Estimation

In order to validate the functionality of the instrument, the objective of this technology demonstration mission is to estimate true anomaly of a small satellite in the Low Earth Orbit (LEO) using the X-ray photon count measurements. The geometry of the problem is shown in figure 5.

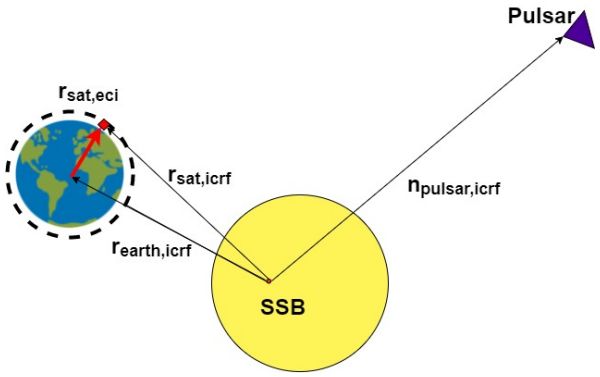

Figure 5: Navigation problem representation

The frame of reference chosen here is the International Celestial Reference Frame (ICRF), which is an inertial frame centered at the Solar System Barycenter (SSB). The value of the dot product of the satellite's position vector ($\vec{r}_{\text{sat,icrf}}$) with the pulsar's position unit vector ($\vec{n}_{\text{pulsar,icrf}}$) can be estimated as follows:

$$\vec{r}_{\text{sat,icrf}} \cdot \vec{n}_{\text{pulsar,icrf}} = c \cdot t_d \tag{5}$$

where c is the speed of light and t_d is the time delay in the pulse profile measured at the satellite with respect to the pulse profile at the SSB. For a typical small satellite orbiting in the LEO, we assume all other orbital elements except true anomaly to remain constant as the satellite propagates in orbit. Thus, equation 5 can be then used to calculate the true anomaly of the satellite, using the measurements from a single pulsar. The procedure of calculating the true anomaly of the satellite, can be broadly divided into two main steps:

- **Step-1:** Generating the time delay (t_d) using the X-ray photon count measurements
- **Step-2:** Using the time delay (t_d) value to estimate true anomaly of the satellite.

This section describes both the steps, and provides details of the mathematics and simulations developed for the same.

Step 1: Estimating t_d using X-ray photon count measurements

As explained in the previous section, the instrument generates time stamped X-ray photon count values. Preliminary analysis shows that, for the Crab pulsar (which is the most appropriate pulsar for this particular mission design, out of all the pulsars considered in the pulsar source catalog) with a 2-10 keV flux[4] of 1.54 photons cm^{-2} s^{-1}, roughly 7.74 $\times 10^{-6}$ photons are detected in a timespan of 1 μs with the proposed detector configuration of 10 SDD detectors and a combined active area of 5 cm^2. This number is useful as an estimate for the average number of photons seen by the detectors, in a time interval corresponding to the desired time resolution of the detectors. It is also useful in deciding the sampling time of the processing electronics.

If the satellite is stationary at one location, with the current instrument configuration it takes an integration time of 100 seconds to accurately determine the pulse profile, as explained in previous sections. However, since the satellite is moving in orbit, the measurements taken at different times correspond to different physical locations. The raw measurements will be first compensated for the movement of the satellite considering the Doppler shift of the pulsar pulse profile due to the satellites velocity. Then epoch folding will be performed on the measurements to obtain the pulse profile at a certain position. Once the pulse profile at a certain location is obtained, it can be compared to the reference pulse profile at the SSB to obtain the time delay t_d.

Step 2: Estimating true anomaly using t_d

To estimate true anomaly, the position of the satellite must be first expressed in the Earth Centered Inertial (ECI) frame. The position of the satellite in ICRF is related to the position of the satellite in ECI frame as follows:

$$\vec{r}_{\text{sat,icrf}} = \vec{r}_{\text{sat,eci}} - \vec{r}_{\text{SSB, eci}} \tag{6}$$

This is because the axes of the ICRF and ECI can be assumed to be oriented in the same direction (neglecting relativistic effects), thus making the coordinate transformation only a translation from the earth center to the solar system barycenter. The vector ($\vec{r}_{\text{ssb,eci}}$) denotes the position of the solar system barycenter in the ECI frame, is a function of time and can be obtained from NASA standard DE430 ephemeris. Using equation 5 and 6, we get:

$$(\vec{r}_{\text{sat,eci}} - \vec{r}_{\text{ssb,eci}}) \cdot \vec{n}_{\text{pulsar,icrf}} = c \cdot t_d \tag{7}$$

If the position of the satellite is unknown, Eq. 5, consists of three unknowns, namely the three components of the satellite's position in ECI frame. As mentioned previously, for this mission, it is assumed that five of the six orbital elements - Semi major axis (a), Eccentricity (e), Argument of perigee, Inclination, Right ascension of ascending node of the small satellite are known. Thus, true anomaly θ of the satellite is the only unknown variable. In order to obtain true anomaly, we need to express the satellites position in the ECI frame in terms of true anomaly. We first express the satellite's position in the orbit frame or the perifocal frame ($\vec{r}_{\text{sat,orbit}}$), in terms of the true anomaly:

$$\vec{r}_{\text{sat,orbit}} = \frac{a \cdot (1 - e^2)}{1 + e \cdot \cos\theta} \cdot \begin{pmatrix} \cos\theta \\ \sin\theta \\ 0 \end{pmatrix} \tag{8}$$

Then we transform this position vector to the ECI frame, as follows:

$$\vec{r}_{\text{sat,eci}} = Q \cdot \vec{r}_{\text{sat,orbit}} \tag{9}$$

where Q denotes the transformation matrix from orbit frame to ECI frame, and is completely determined by the argument of perigee, the right ascension of ascending node and the eccentricity of an orbit. Thus, using equation 8 and 9 we get,

$$\vec{r}_{\text{sat,eci}} = Q \cdot \frac{a \cdot (1 - e^2)}{1 + e \cdot \cos\theta} \cdot \begin{pmatrix} \cos\theta \\ \sin\theta \\ 0 \end{pmatrix} \tag{10}$$

Lastly, substituting the $\vec{r}_{\text{sat,eci}}$ in equation 7, we get:

$$(Q \cdot \frac{a \cdot (1 - e^2)}{1 + e \cdot \cos\theta} \cdot \begin{pmatrix} \cos\theta \\ \sin\theta \\ 0 \end{pmatrix} - \vec{r}_{\text{SSB,eci}}) \cdot \vec{n} = c \cdot t_d \tag{11}$$

Solving these equations for the unknown true anomaly (θ), we get:

$$\theta = n\pi + (-1)^n \sin^{-1}\left(\frac{f(t)}{\sqrt{k_1^2 + k_2^2}}\right) - K_2) \tag{12}$$

where,

$$f(t) = \frac{ct_d - \vec{n} \cdot \vec{r}_{\text{SSB,eci}}}{a \cdot (1 - e^2)} \tag{13}$$

$$K_2 = \sin^{-1}\left(\frac{k_1}{\sqrt{k_1^2 + k_2^2}}\right) \tag{14}$$

and k_1 and k_2 are constants obtained from the matrix transformations. The constant **n** arises from the inverse sine function and can be used to differentiate between the two positions of the satellite that are mirror images about a imaginary line along the pulsar's direction vector, as shown in Fig.6.

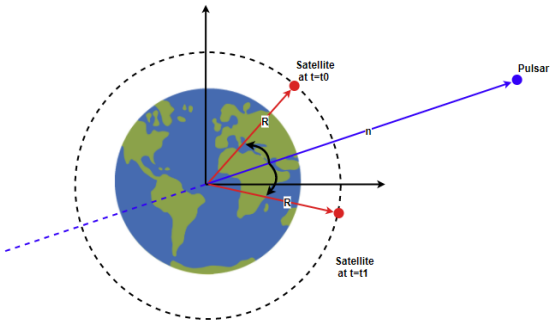

Figure 6: Satellite Mirror Image Positions

The value of **n** will be determined using the Doppler effect observed in the sensor measurements and can be used to differentiate between the two mirror image positions. Depending on the value of $\vec{v}_e \cdot \vec{n}$, where $\vec{v}_e$ denotes the velocity of the satellite in ECI frame, the value of the true anomaly can be estimated as follows:

$$\theta = \begin{cases} \sin^{-1}\frac{f(t)}{\sqrt{k_1^2+k_2^2}} - K_2 & \text{if } \vec{v_e} \cdot \vec{n} > 0 \\ \pi - \sin^{-1}\frac{f(t)}{\sqrt{k_1^2+k_2^2}} - K_2 & \text{if } \vec{v_e} \cdot \vec{n} < 0 \end{cases} \tag{15}$$

Thus, we have derived a mathematical relation for estimating the true anomaly of the satellite only using the time delay (t_d) value estimated from the X-ray photon measurements.

Simulation and Validation

A simulation was setup to validate the derived formula for true anomaly estimation and to predict the expected error range. The simulation uses a orbit propagator from the open-source Python library Poliastro[11] which propagates the satellite's orbit in the LEO. At different location in the orbit, the value of t_d was estimated using a reverse engineered formula for t_d as shown in equation 16. In actual flight, this value of t_d would be obtained from instrument's X-ray photon count measurements, as explained in the step 1. The simulated value of t_d, as the satellite propagates in orbit is shown in Figure 7. Gaussian noise was also added to the t_d value so as to simulate in-orbit errors, with a standard deviation of 10 microseconds.

$$t_d = \frac{\vec{r}_{\text{icrf}} \cdot \vec{n}_{\text{icrf}}}{c} \tag{16}$$

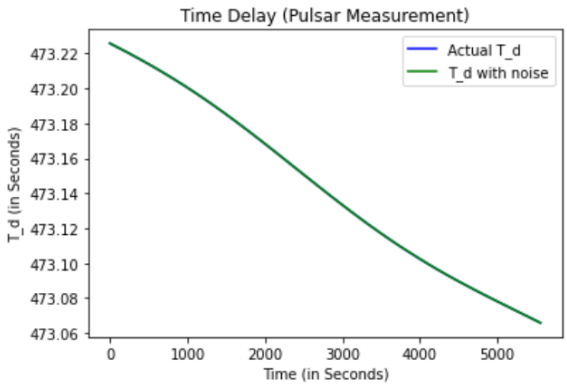

Figure 7: Simulated t_d in Orbit

The t_d values so obtained were used to calculate the true anomaly using the formula derived in the previous section. Shown in Fig. 8 is a plot showing the actual true anomaly (propagated using poliastro) and estimated true anomaly determined using the formula derived. The results validate the derivation of the formula, as simulated true anomaly and calculated true anomaly match closely, with an average error of less than 1 degree. It is observed that the true anomaly error spikes to around 4 degrees at the locations where the satellite crosses the pulsar vector in the ECI frame. Further analysis is being carried out to understand the cause of this error and the steps that can be taken to reduce it.

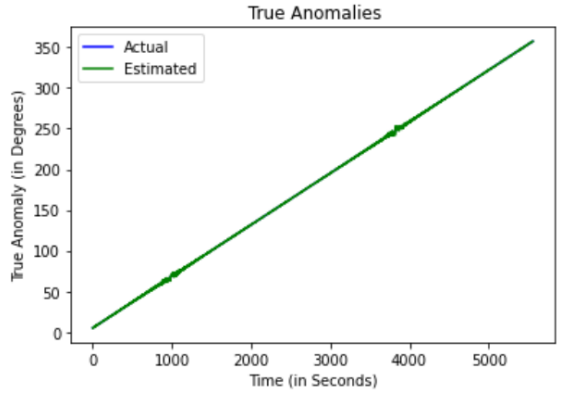

Figure 8: Estimated and Calculated True Anomaly

Mission Design and Concept of Operations

Since this is a technology demonstration mission, the XRay Pulsar navigation will only be conducted during the eclipse duration of the orbit. Figure 9 shows the operational modes of the satellite, between which the satellite transitions based on battery State of Charge (SoC). During the insolated part of the orbit the satellite primarily will point towards the sun to charge the batteries. On entering eclipse, the ADCS system will point the instrument towards the pulsar to take measurements. The measurements from the pulsar (time tagged x-ray photon count values) are stored in the on-board memory of the satellite, until they can be downlinked. Along with the measurements, GPS location of the satellite will also be downlinked so that the true anomaly estimated using instrument measurements can be verified with the actual true anomaly. A 500 km Low Earth Orbit was chosen for the mission with an inclination of 97.8 degrees. Such orbits can be easily provided by the Polar Satellite Launch Vehicle, which is the primary launch vehicle chosen to deploy this satellite. As described in the source selection for X-ray Pulsar Navigation section, choosing this orbit provides high visibility time of the Pulsar, without obstruction by other bright sources. In addition, a near sun synchronous orbit leads to more insolation time, that aids the design of the power system of the satellite.

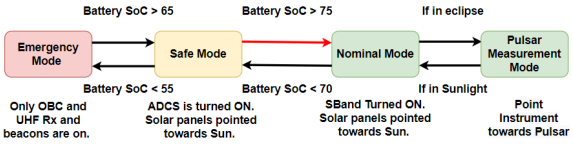

Figure 9: Mode Flow Diagram

Satellite Overview

The XNavSat mission is developed in a 6U form factor with approximate dimensions of 30 cm × 20 cm × 10 cm. Figure 10 shows a preliminary CAD model of the satellite indicating the location of different subsystems in the satellite. The instrument is placed on the -z face of the satellite, occupying around 2U of volume. The spacecraft avionics stack consists of five PC104 standard PCBs which are the On Board Computer, Electrical Power System, UHF Transceiver, S Band Transmitter and Interface Card. The power system of the satellite also consists of a battery pack, placed below the avionics stack and body mounted solar panels on all four faces of the satellite. The Attitude Determination and Control System (ADCS) of the satellite is placed near the +z face of the satellite, which is used to provide 3-axis attitude control of the satellite. A GPS receiver with a patch antenna is also placed on the +z face of the satellite. The antenna deployment module, containing a UHF quaterwave monopole antenna is placed near +z face and is connected to the UHF

transceiver through a SMA harness. The +y face of the satellite consists of the S-Band patch antenna. The UHF and S-Band antennas are placed in this configuration, to ensure that the antennas have significant gain with the groundstation, while the satellite is pointing the solar panels towards the sun during nominal operations.

Figure 11, provides a system level block diagram of the entire satellite showing the interconnections between the different subsystems. In order to realize the mission objectives, the XNavSat mission uses a combination of in-house developed and commercially developed subsystems. The in-house developed subsystems (namely OBC, EPS and structures) derive heritage from the previous Ahan and INSPIRE small satellite missions developed at IIST. The COTS (commercial off the shelf) subsystems, which are the ADCS, UHF Transceiver, S-Band Transmitter and GPS receiver are chosen considering the size, power and cost parameters which are most suitable for the mission. The OBC, EPS, UHF transceiver and S-Band transmitter are connected to each other using the PC104 standard CubeSat bus. This avionics stack, also has an interface card that consists of connectors that are used to connect to the remaining subsystems via harnesses. This section gives a brief overview of the various subsystems and describes their key features.

On Board Computer

The On Board Computer is built around the SmartFusion2 M2S090 SoC (System on Chip) FPGA which incorporates ARM Cortex M3 microprocessor, SRAM (Static RAM), eNVM (electronic nonvolatile memory), RTC (real time counter) and various other features. Since the Microsemi SmartFusion2 SoC FPGAs and IGLOO2 FPGAs are 65 nm, non-volatile, flash-based FPGAs, they exhibit intrinsic robustness against radiation induced single event upsets. The designed board requires a 3.3V supply line to work and the hardware also includes one SD card slot, one 64 Mb SPI-Flash, one ADC, an external processor supervisor circuit and a 9-axis IMU. The 9-axis IMU will be used in the mission for determining the angular rates of the satellite. In-order to make the SoC isolated from the other subsystems of the satellite, Power and Signal Isolators have been used between the SoC and the other subsystems. Figure 12(a) shows the engineering model of the OBC developed, which is currently undergoing comprehensive performance tests to ensure robust functionality. The OBC is responsible for collecting Housekeeping (HK) data from all subsystems and science data from the payload. It is also responsible to implement the flight software and sequence of operations of the satellite while maintaining the appropriate timing requirements.

Communication System

The primary groundstation for the mission will be the UHF and S-Band groundstation established at IIST. An access time analysis was performed to estimate the total number of passes and the link time the satellite has with the groundstation. The satellite contains a UHF transceiver with a data rate of 9600 bps (more details of which are given in the subsequent section), using which an average 720 kilobytes of data can be downlinked to earth per day. The UHF link will be mainly used to downlink satellite housekeeping telemetry. The satellite also contains a S-Band Transmitter with a data rate of 2 Mbps that will be used to downlink the science instrument data.

Figure 12(b), shows the engineering model of the UHF transceiver board developed. The communication system uses a COTS UHF half-duplex transceiver developed by NanoAvionics with a proposed operating frequency of 437 MHz. Since the UHF transceiver would be mainly used for transmitting small-sized beacons to the ground-station, an antenna with high directivity is not required. It is further essential that beacon transmissions are not dependent on the pointing ability of the satellite, thus there is a need for the gain pattern of the antenna to be omnidirectional. Thus, a monopole tape measure antenna was chosen. The tape measure antenna is housed in an Antenna Deployments Module (ADM), which uses a burn-wire deployment mechanism that derives heritage from the INSPIRESat-4[12] small satellite mission. A link budget analysis was also performed that ensures the feasibility of the UHF and S-Band based communication system for the mission.

Electrical Power System

The electrical power system of the satellite consists of a charger board, a battery board and four solar panels. The satellite consists of four body-mounted solar panels which have AzureSpace 3G30A cells. The panels on the +x and -x faces of the satellite consist of 14 solar cells each, and the panels on +y and -y face consists of 7 solar cells each. The amount of time the satellite will be in isolation and in eclipse was simulated using the Systems Tool Kit (STK) student version software. According to the analysis, an average of 28 minutes of eclipse time will

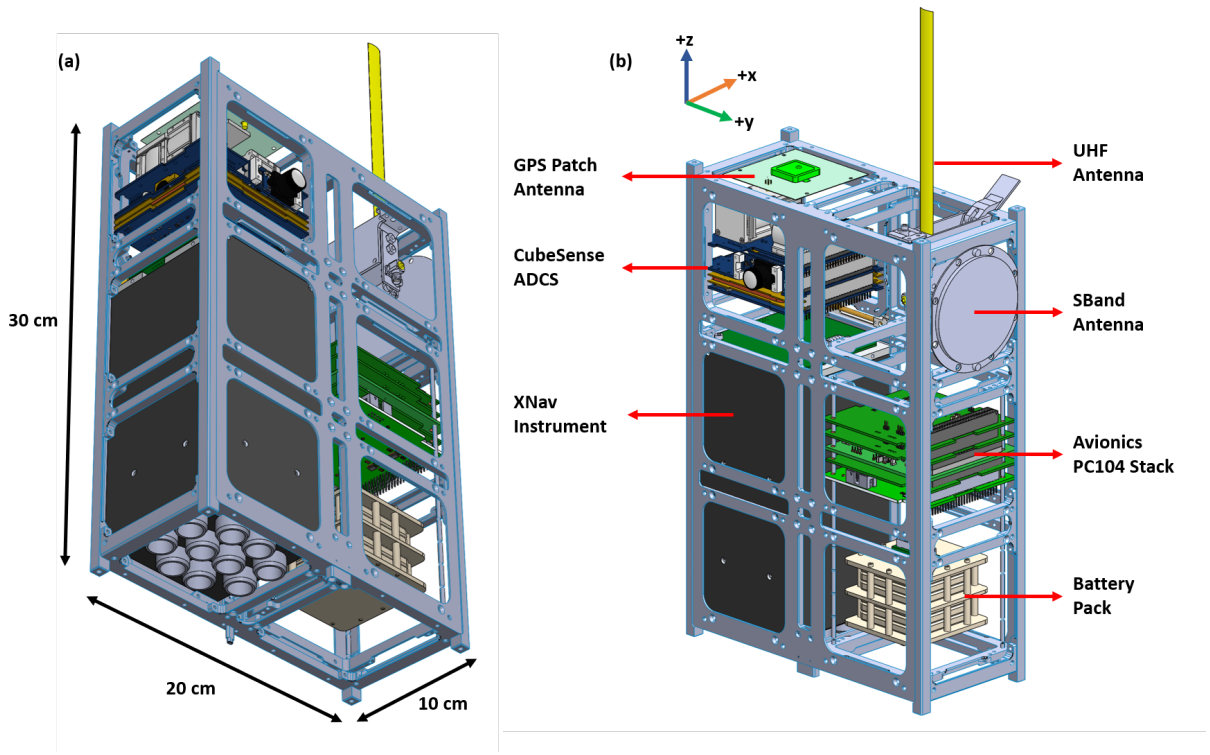

Figure 10: Satellite Preliminary CAD Model

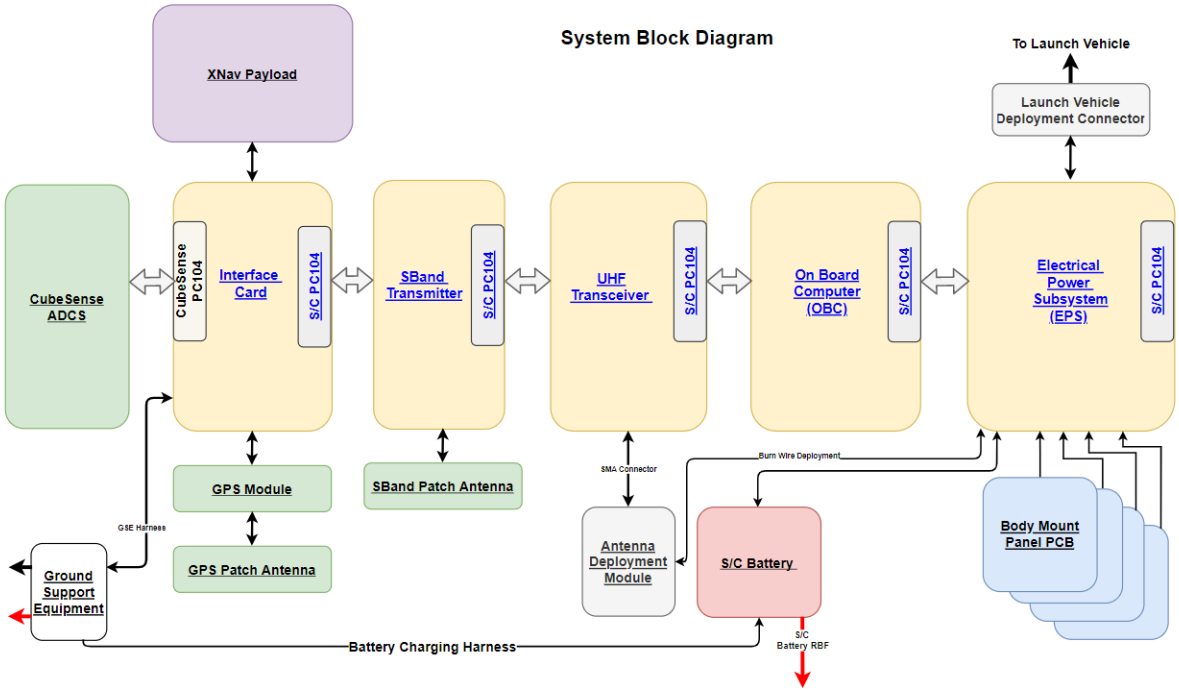

Figure 11: System Block Diagram

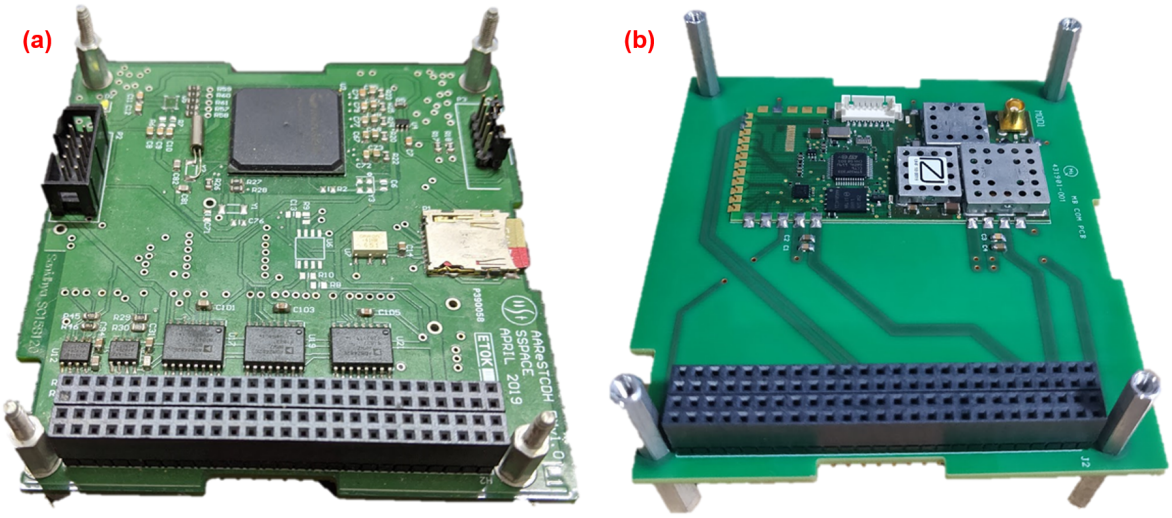

Figure 12: Mission Avionics EMs: (a) OBC (b) UHF Transceiver

be seen per orbit with a maximum eclipse duration of 30 minutes. As mentioned in the previous section, the satellite will point towards the sun during the insolated part of the orbit. Assuming the +x or -x directly pointed towards the sun, approximately 14.3 Watts of instantaneous power will be generated. Preliminary power requirements of the satellite, indicate that the duty-cycled peak power consumption of the satellite is approximately 11 Watts. Based on the power consumption and power generation of the satellite, in-order to ensure a maximum SoC drop of 30%, the battery capacity was chosen. The battery pack consists of four Lithium ion LG 18650HE2 cells in a 2S-2P configuration, generating a nominal battery voltage of 7.2 volts and a nominal battery capacity of 5000 mAh. The charger board is designed to charge the batteries using the solar panels and also provide regulated power to the various subsystems of the small satellite.

Attitude determination and Control System

In order to point the instrument towards a pulsar, a highly accurate commercial of the shelf ADCS made by CubeSpace is chosen for the mission. The ADCS contains a variety of sensors including a fine and coarse sun sensors, nadir sensors as well as a star tracker using which it can achieve an attitude measurement accuracy of 0.1 degrees. The ADCS contains three reaction wheels and three magnetorquers and is capable of 3 axis pointing with a pointing accuracy of 0.2 degrees. With all components included, the size of the system is around 1U and is placed on the +z face of the satellite.

Conclusion

This article describes the design of a small-satellite mission to demonstrate true anomaly determination of a LEO satellite using millisecond X-ray pulsar timing measurements. Procedure for selecting the most appropriate pulsar source along with the expected signal to noise ratio at the detector was developed. A preliminary design for a instrument to extract timing information from X-ray photons has also been completed. An algorithm for calculating the satellite's true anomaly based on X-Ray pulsar timing measurements has been developed along with simulation results. The article concludes with an overview of the small satellite system design for this mission. A successful demonstration will the pave the way for future small satellite missions to use X-Ray Pulsars for autonomous navigation in space.

Acknowledgements

We thank all members of the Small-spacecraft Systems and PAyload CEntre (SSPACE) for their support in the development of the mission. In particular we acknowledge the contributions of Devashish Bhalla and Dhruva Anantha Datta in the development of the satellite. We would like to thank Dr. Umesh R. Khadane for his inputs on the instrument signal conditioning circuit design. SSPACE is a part of the INSPIRE international consortium, and we acknowledge the INSPIRE partner universities for their knowledge transfer of small satellite systems engineering and development.

References

[1] T. J. Chester and S. A. Butman, "Navigation Using X-Ray Pulsars," *Telecommunications and Data Acquisition Progress Report*, vol. 63, pp. 22–25, Mar. 1981.

[2] *SEXTANT X-ray Pulsar Navigation demonstration: Flight system and test results.* 2016 IEEE Aerospace Conference, 03 2016.

[3] J. Taylor, "Millisecond pulsars: nature's most stable clocks," *Proceedings of the IEEE*, vol. 79, no. 7, pp. 1054–1062, Jul. 1991. [Online]. Available: https://doi.org/10.1109/5.84982

[4] S. I. Sheikh, "The use of variable celestial x-ray sources for spacecraft navigation," Ph.D. dissertation, University of Maryland, 2005.

[5] F. Bonnarel, P. Fernique, O. Bienaymé, D. Egret, F. Genova, M. Louys, F. Ochsenbein, M. Wenger, and J. G. Bartlett, "The ALADIN interactive sky atlas," *Astronomy and Astrophysics Supplement Series*, vol. 143, no. 1, pp. 33–40, Apr. 2000. [Online]. Available: https://doi.org/10.1051/aas:2000331

[6] S. Rosen, "VizieR Online Data Catalog: Enhanced 3XMM catalogue (3XMMe) (Rosen+, 2016)," *VizieR Online Data Catalog*, p. IX/47, Apr. 2016.

[7] I. N. Evans, C. Allen, C. S. Anderson, J. A. Budynkiewicz, D. Burke, J. Chen, F. Civano, R. D'Abrusco, S. M. Doe, J. D. Evans, G. Fabbiano, D. G. Gibbs, K. J. Glotfelty, D. E. Graessle, J. D. Grier, R. Hain, D. M. Hall, P. N. Harbo, J. C. Houck, J. Lauer, O. Laurino, N. P. Lee, R. Martinez-Galarza, M. L. McCollough, J. C. McDowell, J. Miller, W. McLaughlin, D. L. Morgan, A. E. Mossman, D. T. Nguyen, J. S. Nichols, M. Nowak, C. Paxson, D. A. Plummer, F. A. Primini, A. H. Rots, A. Siemiginowska, B. A. Sundheim, M. S. Tibbetts, D. W. Van Stone, and P. Zografou, "Chandra Source Catalog Release 2.0 - The State of the Art Serendipitous X-ray Source Catalog," in *AAS/High Energy Astrophysics Division*, ser. AAS/High Energy Astrophysics Division, vol. 17, Mar. 2019, p. 114.01.

[8] I. N. Evans, F. A. Primini, J. B. Miller, J. D. Evans, C. E. Allen, C. S. Anderson, G. Becker, J. A. Budynkiewicz, D. Burke, J. C. Chen, F. Civano, R. D'Abrusco, S. M. Doe, G. Fabbiano, J. Martinez Galarza, I. Gibbs, D. G., K. J. Glotfelty, D. E. Graessle, J. Grier, J. D., R. M. Hain, D. M. Hall, P. N. Harbo, J. C. Houck, J. L. Lauer, O. Laurino, N. P. Lee, M. L. McCollough, J. C. McDowell, W. McLaughlin, D. L. Morgan, A. E. Mossman, D. T. Nguyen, J. S. Nichols, M. A. Nowak, C. Paxson, M. Perdikeas, D. A. Plummer, A. H. Rots, A. L. Siemiginowska, B. A. Sundheim, S. Thong, M. S. Tibbetts, D. W. Van Stone, S. L. Winkelman, and P. Zografou, "The Chandra Source Catalog — A Billion X-ray Photons," in *American Astronomical Society Meeting Abstracts #235*, ser. American Astronomical Society Meeting Abstracts, vol. 235, Jan. 2020, p. 154.05.

[9] W. Voges, B. Aschenbach, T. Boller, H. Brauninger, U. Briel, W. Burkert, K. Dennerl, J. Englhauser, R. Gruber, F. Haberl, G. Hartner, G. Hasinger, E. Pfeffermann, W. Pietsch, P. Predehl, J. Schmitt, J. Trumper, and U. Zimmermann, "Rosat All-Sky Survey Faint Source Catalogue," *IAU Circular*, vol. 7432, p. 3, May 2000.

[10] Amptek. Amptek 70 mm² FAST SDD® – x-ray detectors and electronics. [Online]. Available: https://www.amptek.com/internal-products/70-mm2-fast-sdd

[11] J. L. C. Rodríguez, M. Jorge, A. Hidalgo, Shreyas Bapat, N. Astrakhantsev, Chatziargyriou Eleftheria, Meu, , Dani, Abhishek Chaurasia, Yash-10, A. L. Márquez, Dhruv Sondhi, Tomek Mrugalski, E. Selwood, Orestis Ousoultzoglou, P. R. Robles, G. Lindahl, Andrea-Carballo, A. Rode, H. Eichhorn, Himanshu Garg, Hrishikesh Goyal, I. Des-Jardin, AOrionis, AntoniiaK, Josvth, Priyanshu Rohilla, Angala, O. Streicher, and R. A. Lehmkuhl, "poliastro/poliastro: poliastro 0.15.0 (earth edition)," 2021. [Online]. Available: https://zenodo.org/record/4763538

[12] S. Sarthak, T. K. Anant Kumar, and G. F. Gacal, "Inspiresat-4 / arcade: A vleo mission for atmospheric temperature measurements and ionospheric plasma characterization," in *Proceedings of the 33rd Annual AIAA/USU Small Satellite Conference, Session VIII: Frank J. Reed Student Competition, SSC19-V-06*, Utah, USA, 2019.